Раздел второй

ФИЗИКА И ТЕХНОЛОГИЯ КОНСТРУКЦИОННЫХ МАТЕРИАЛОВ

ELECTRON IRRADIATION, TEMPERATURE, AND STRESS EFFECT ON CORROSION OF Zr-, Ni-Cr-, AND Fe-Cr-BASED ALLOYS IN THE VICINITY OF THE WATER COOLANT SUPERCRITICAL TRANSITION

O.S. Bakai, V.M. Boriskin, M.I. Bratchenko, S.V. Dyuldya
National Science Center "Kharkov Institute of Physics and Technology", Kharkiv, Ukraine
E-mail: bakai@kipt.kharkov.ua

Quantitative regularities of the Zr-1%Nb alloy, Ni-Cr alloy 690 and Fr-Cr stainless steel (SS) 12X18H10T corrosion in the near-critical domain (23.5 MPa, 360…380 °C) of a circulating water coolant are searched using multi-scale calculations of the NSC KIPT Super-Critical Water (SCW) Convection Loop experiment *e*-irradiation environment qualifiers. The per-sample quantification of irradiation doses, temperatures, stress, and the radiolytically altered coolant chemistry was obtained. A bi-linear increase of the oxidized coupons weight gain with absorbed dose and corrodent temperature has been first revealed and described within the proposed mechanistic model approach. The origin of the experimentally found corrosion cracking of the SS sample has been attributed to the irradiation induced thermal-elastic hoop stress. The cracks activation threshold stress is predicted to lie between 40 and 80 MPa. An experimental technique to study the controlled stress governed corrosion in SCW under irradiation is presented.

PACS: 81.40.Np;81.65.Mq;78.66.Bz;61.82.-d;61.80.Fe;82.50.Kx;82.33.De;44.25.+f;65.40.De;07.05.Tp

INTRODUCTION

Corrosion of alloys in chemically aggressive hot coolants (such as a pressurized sub- and Super-Critical Water (SCW) or molten salts) under reactor (n, γ)-irradiation is an essential determinative of the structural materials performance and safety [1, 2]. An irradiation impact on corrosion resistance is so far unclear (at least quantitatively) and is hard to be studied in-pile, especially with reference to innovative Generation IV reactors. Accelerator simulation irradiation [3] and advanced multi-scale computer modeling [4] both belong to a valuable cost-effective roadmap to identify the corrosion behavior driving forces and regularities as well as the methods of its control by means of high-purity alloying and surface engineering. Particularly, the NSC KIPT LEA-10 linac based Electron Irradiation Test Facility (E.I.T.F.) is applied for assessment of advanced structural materials of the GenIV SCW cooled reactor, SCWR, by means of the dedicated circulation loop with water in sub- and super-critical states. The E.I.T.F. unique methodology [5] of *in situ* (e^-, γ)-irradiation provides research of Irradiation Assisted Corrosion (IAC) and Irradiation Assisted Stress Corrosion Cracking (IASCC) [6, 7]. As well, R&D of the Irradiation Assisted Fatigue Corrosion, IAFC, studies technique is in progress.

An extensive set of the NSC KIPT E.I.T.F. priority experimental data [6] on Zr- and, Ni-Cr-based alloys and Fe-Cr austenitic stainless steel (SS) IAC/IASCC in the vicinity of water coolant flow super-critical transition is still subjected to post-irradiation studies [7, 8]. Though the irradiation induced enhancement of alloys oxidation/corrosion rate had been clearly established in ref. [6] and has been confirmed afterwards at a high-resolution analysis of the specimens microstructure [7], the effect qualification with a kind of predictive quantitative model description has not been elaborated up-to-date. This is the goal of the present paper which is specifically focused on the theoretical insight on the post-irradiation examination data base on the Multi-Scale Modeling & Simulation (MSMS) technique [4].

The paper is organized as follows. In Section 2, we start with a brief survey of the facility [6], the investigated materials and the obtained experimental responses [7], identify the issues of their elucidation and formulate the explicit task of this work. The MSMS procedure applied to solve it is given in Section 3. It is followed their by the results of coupled calculations of the E.I.T.F. irradiation [6] relevant thermal hydraulics, dosimetry, coolant radiolysis and thermal and stress-strain state of materials. Section 4 comprises application of these data to the analysis of experimental [6, 7] observables. In Section 4.1, the IAC empirical regularities are revealed and discussed; the phenomenological model approach to their systematics is also introduced. The physical reason of the observed IASCC is identified in Section 4.2. The overall conclusions and the prospects of further R&D are summarized in the final Section 5.

1. THE NSC KIPT E.I.T.F. EXPERIMENTAL

1.1. FACILITY AND IRRADIATION SETUP

An *in situ* e^--irradiation of samples of materials is carried out at the circulation loop, SCWNCL (Fig. 1), specially designed to conduct experiments in a broad neighborhood (350…400 °C) of the water critical point (P_c, T_c) = (22.064 MPa, 374 °C) under 10 MeV/10 kW_e scanning electron beam (EB) of the LEA-10 linac.

The loop operates according to the coolant natural convection principle: water is heated by electric heaters (as well as by the EB power deposition) and floats up due to decrease of density ρ and the correspondent increase in buoyancy. The steady-state circulation at a constant mass-flow rate W is provided with coolers; W is determined by a balance of heating and cooling effects.

Specimens, in the form of thin rectangular plates, are put into the 4-channel irradiation cell, IC (see Fig. 1) which grants practically complete absorption of EB power in the IC tubes and specimens. Due to gradual slowing down of electrons and unevenness of the scanning EB coverage of samples, different ones absorb different doses[1] $D = (N_A/M)\cdot E_{dep}$.

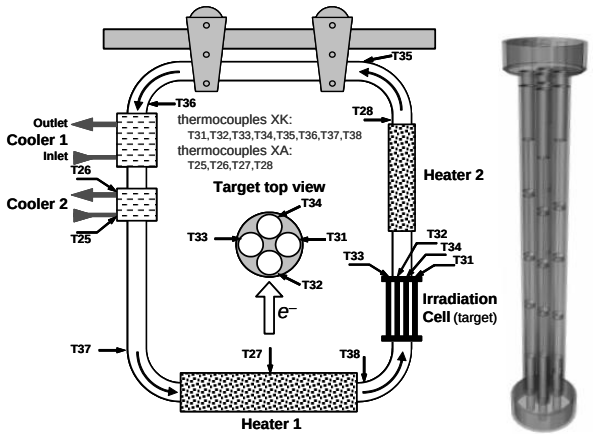

Fig. 1. Schematics of the E.I.T.F. SCW Natural Circulation Loop (SCWNCL) and its target four-channel target Irradiation Cell (IC)

At a steady-state irradiation regime, samples also differ by their temperatures T_s and by the temperature T_w, density $\rho(P, T_w)$ and velocity v of surrounding convective flow of corrosive coolant. This allows attribution of corrosion responses to a rather wide range of doses and temperatures within the same irradiation session. From the other hand, this impedes their quantitative analysis since all these corrosion control parameters are practically inaccessible for direct *per sample* measurements inside the IC irradiation zone. We overcome this inevitable experimental obstacle by the application of a sophisticated computer model of the facility operation at each specific irradiation protocol.

The LEU-10 MeV/10 kW e^--irradiation load is high: the Total Ionization Dose (TID) rate $\dot{D}$ amounts to ~ 15…30 kGy/s in samples and ~ 5…10 kGy/s in a coolant. This is ~ $10^{1...2}$ times greater than the corrosion affecting γ-heating rate in a reactor. Thus, E.I.T.F. is capable of express simulation of the SCWR candidate materials corrosion scenarios at samples exposure less than 10^3 h.

Below we confine ourselves to the pioneering (2012) 497 h-long E.I.T.F. irradiation experiment [6, 7]. It dealt with three kinds of tested materials: the cladding Zirconium based alloy and the vessel/piping materials, the corrosion-resistant Inconel™ grade Ni-Cr alloys and the 12X18H10T steel. Except of the latter one, which was an industrial SS used for the loop piping and IC manufacturing, the sample coupons' materials were intentionally fabricated, in different institutions, from high-purity (99.9999 at.%) components.

The Zr-1%Nb alloy (6.5 g/cm^3) was designed and fabricated in the NSC KIPT Institute for Material Science and Technologies. Eight 40×9×0.5 mm sized coupons ##1–8 were manufactured.

Other eight coupons (50×9×1.2 mm, 8.19 g/cm^3) were fabricated from Ni-Cr alloys. Each of them was made, in the Kyiv Paton Institute of Electric Welding, as a combination of two materials of the same family but of different chemistry. The base material, alloy 690

$$Ni_{(base)}Cr_{32.4}Fe_{9.55}Ti_{0.35}C_{0.14at.\%},$$

was welded, in the coupon mid-portion, with the auxiliary innovative alloy In 52 MSS

$$Ni_{(base)}Cr_{29.6}Fe_8Mo_{1.8}Nb_{1.5}Mn_{0.18}Si_{0.31}Ti_{0.17}C_{0.1at.\%}.$$

The difference of corrosion behavior of these materials and effects' features located in the vicinity of the welding joint were of special interest.

Sixteen coupons were mounted in different IC tubes to obtain different irradiation loads. Particularly, coupons No 7, 8 of each material were placed inside the rear (*wrt.* the linac e^--beam) IC tube No IV. Due to the EB absorption, the flux of primary electrons was negligible inside these samples which were only weakly γ-irradiated by the EB bremsstrahlung and thus played a role of 'witness' samples *wrt.* the much highly irradiated coupons in other tubes of the IC.

The SS 12X18H10T samples were, in fact, the annular rings cut, after irradiation completed, from the bottom and top parts of the sample holding cartridge of the most highly irradiated frontal IC tube No II.

Coupons were exposed, *in toto* during 560 h, to the deoxygenated water coolant with pH = 6.5 in the vicinity of the water pseudo-critical point $T_{pc}(P)$ = 379.5 °C of the SCWNCL pressurized to P = 23.5 MPa. The water coolant circulation characteristic[2] mass-flow rate was W = 60 g/s. Inclusively during 497 h, they were irradiated by the KIPT LUE-10 linac 9…11 MeV e^--beam of 9.76 MeV mean energy $\langle E_e \rangle$, 0.5…0.8 μA mean current $\langle I \rangle$, 6.23 kW$_e$ mean power $\langle Q_e \rangle$, 3.4 μs EB pulse duration at 250 Hz repetition rate, and 3.5 Hz EB scanning frequency. The total fluence amounted to ~10^{21} e^-/cm^2.

1.2. THE EXPERIMENTAL DATA

Immediately after removal from the IC cartridges, all the coupons were subjected to General Corrosion Test (GCT) of specific weight/loss (WG/WL, per surface unit area) $\delta m/S$ measurement by means of a Class 2 (± 0.15 mg) laboratory equal-arm balance VLR-200 [6]. The obtained results are depicted in Fig. 2.

[1] E_{dep} is the dose D equivalent specific energy, keV per atom, deposited by e^--beam in a material having mean atomic mass M, N_A is the Avogadro number.

[2] A somewhat greater value W = 80 g/s was reported in [6, 7] base on a limited set of dedicated test measurements. The currently adopted value, 60 g/s, follows from the refined calculation of the samples loaded IC hydraulic resistance.

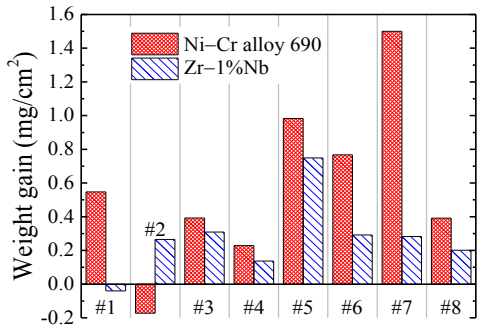

Fig. 2. Specific weight gain/loss δm/S and estimated oxidation/corrosion layer thickness h_{ox} of (e^-, γ) irradiated coupons of Zr- and Ni-Cr-based alloys [6]

Other post-irradiation studies resulted in characterization of the corrosion layer microstructure, microhardness and chemistry of selected specimens and samples of the IC material by means of optical metallography, SEM/STEM EDS/AES and FIB instrumentation of several labs. The results are given and discussed in ref. [7].

One of them consists in the observed Inter-Granular SCC (IGSCC) of welding joint areas of Inconel samples as well as of the highly irradiated sample of the SS IC piping. It was rather unlooked-for since no stress load was intentionally applied within the experimental setup. In ref. [7], the nature of the IGSCC was only qualitatively attributed to the welding residual stress and the irradiation assisted thermal-elastic stress, respectively. The quantitative description of the latter effect is definitely required, and we address this problem in Section 4.2.

Returning to the IAC GCT results of Fig. 2, we draw attention to the very notable variability of WG/WL data for samples of each material. For Zr alloy coupons, the mean value $\langle \delta m/S \rangle = 0.27$ at 0.22 mg/cm^2 r.m.s. deviation. As well, $\langle \delta m/S \rangle = (0.58 \pm 0.51)$ mg/cm^2 for Inconel coupons. In both cases, the 'variance-to-mean' ratios tend to 100%. However, statistical tests decline the hypothesis of Gaussian distribution of these data scattering up to 95% confidence level. This points to existence of hidden regularities of the IAC data. The task arises to qualify them with generally poorly experimentally identifiable quantitative parameters (dose rate, temperature, *etc.*) of the SCWNCL IC e^--irradiation environment each of the samples was corroded in. Our advances in revealing of these regularities are presented in Section. 4.1.

1.3. CHALLENGES & PROBLEM STATEMENT

In is worth noting here that our early attempts [6] to find rather simple dependency of GCT data on dose or temperature base on preliminary characterization of irradiation experiment have not been successful. Huge scattering of WG(E_{dep}) and WG(max T_s) is evident in Fig. 3. Only certain (still doubtful) correlation of oxidation rate to max $T_s > T_{pc}$ is peeking in this figure. No quantitative (and even qualitative) scaling of oxidation rate with the expected dose load variable E_{dep} is observed. From the point of view of radiation physics and Radiation Material Science (RMS) trends [2], this looks odd.

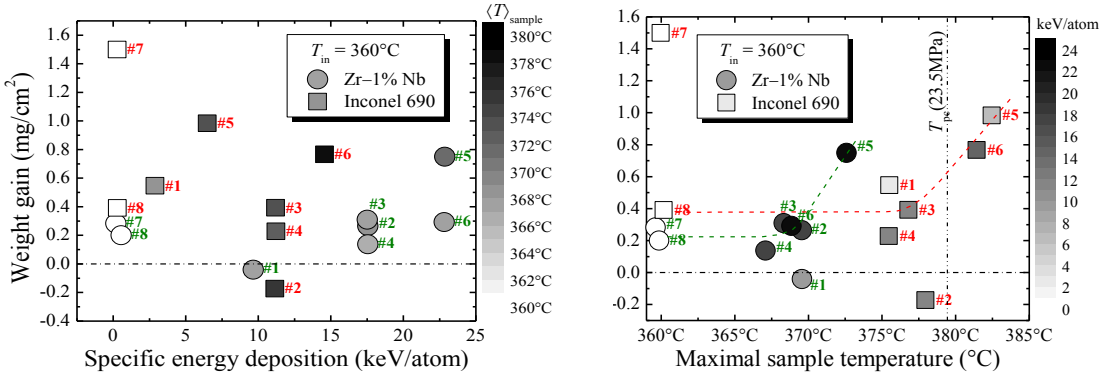

Fig. 3. Scatter plots of the measured δm/S of Fig. 2 vs. the calculated E_{dep} and the maximal T_s of samples [6]

The reason of this oddness is found in fundamentals of corrosion science [9, 10, 1]. Corrosion is a multifactorial physical-chemical phenomenon coherently affected by multiple mutually connected driving forces and control variables (Fig. 4). When a certain of them is (somewhat randomly) assigned as a primary one[1], the co-operative effect of other, indirect, driving forces is not negligible. The non-linear dependency between these entities is generally strong, *esp.* under irradiation, i.e. just in the case of the E.I.T.F. experiment.

In brief, this paradigm can be clarified by the Fig. 4 graph interlinks. Let us treat the absorbed dose rate of samples as the problem-specific primary control variable of the E.I.T.F. irradiation which directly activates chemical reactions at the coolant/material interface. The dpa rate (*e.g.*, in a protective oxide layer) is a complementary primary qualifier, though it is weak in E.I.T.F. Suppose other variables fixed, one expects positive correlation of the corrosion rate to either of these ones.

However, irradiation dose rate and power deposition lead to (i) water radiolysis and (ii) local heating of both samples and coolant. Radiolysis results in both short-lived chemically aggressive radicals (this directly affects corrosion rate by emerging a number of irradiation specific volatile reactants) and, at a much longer timescale,

[1] For example, dose and number of atomic displacements per atom, dpa, are common primary control variables of RMS concepts [2] while temperature and corrodent chemistry are most familiar to general corrosion engineering studies [9].

modifies the initial chemistry of coolant by accumulation of quasi-stable reactable products. Changes of temperature, in turn, enhance the Arrhenius-type rates of all chemical reactions; this also indirectly affects the chemistry of water. Besides, inevitable temperature gradients result in thermal-elastic stress which can range up to the activation of IASCC. Fast circulation of coolant promotes the Flow Accelerated Corrosion (FAC [9, 10]) effects absent in static autoclaves. For the same thermal hydraulics and hydrodynamic reasons, the temperatures of coolant and samples generally differ since they cannot reach thermodynamic equilibrium replaced by a circulation loop specific balance of heat generation, transfer, and loss. Indirectly, this tunes non-linearly the temperature distributions, affects reaction rates (and, thus, water chemistry), and even can induce very specific thermal-elastic effects at interfaces.

The observed GCT responses [6] of Fig. 2 has been formed under combined impact of all these agents. Each of them contributes to the observables in its own, generally unknown, extent. Because of their interlinking and co-variation, needless to expect the applicability of single-parameter models (like those searched in Fig. 3) for quantitative description of GCT data. Instead, co-operative co-dependent multi-parametric models are required to rationalize them and to uncover the essence of the first observed [6] irradiation effect on corrosion rate.

This is just the problem we ventured to solve in the present study. The question arose: how to identify the most relevant control variables to fit the experimental data with? Taking into account very different length and time scales of co-operatively playing processes, we have chosen MSMS as the only tool suitable to answer it.

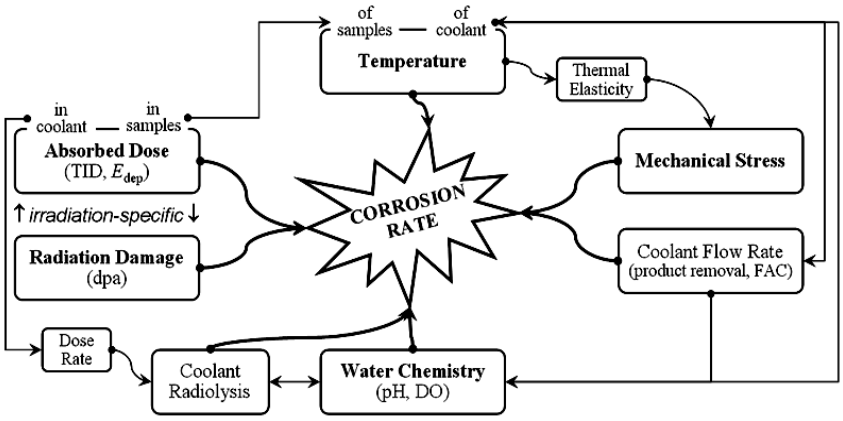

Fig. 4. Interconnected driving forces and control variables of the materials corrosion in conditions of the E.I.T.F. SCWNCL irradiation experiment

2. MULTISCALE MODELING PROCEDURE

The adopted MSMS workflow [11] is depicted in a (to some extent simplified) diagram of Fig. 5.

We start with the System Thermal Hydraulic (STH) qualification of the coolant steady-state circulation. It is obtained by means of the NSC KIPT developed E.I.T.F. SCWNCL specific 1D STH code [12]. The simulation is iterative since STH is affected by the EB power deposition in samples and coolant which is simulated, in 3D, using the GEANT4 Toolkit based Monte Carlo (MC) radiation transport (RT) code RaT 3.1 [13]. This in-house developed code is also applied to the high-resolution computational dosimetry of samples (dose, dpa) and simulation of the initial stages of water radiolysis kinetics. The consistent calculations of temperature and stress fields is performed using the Finite Element Method (FEM) software FreeFEM++ [14]. All these outputs are transferred to inputs of numerical, semi-analytic phenomenological and kinetic Monte Carlo (kMC) models of radiolysis and oxidation kinetics (*e.g.*, by means of the kMC code SPPARKS [15]) to estimate the corrosion responses of interest. Below in this section, we present only the major results of MSMS without going into the fine details of the calculations.

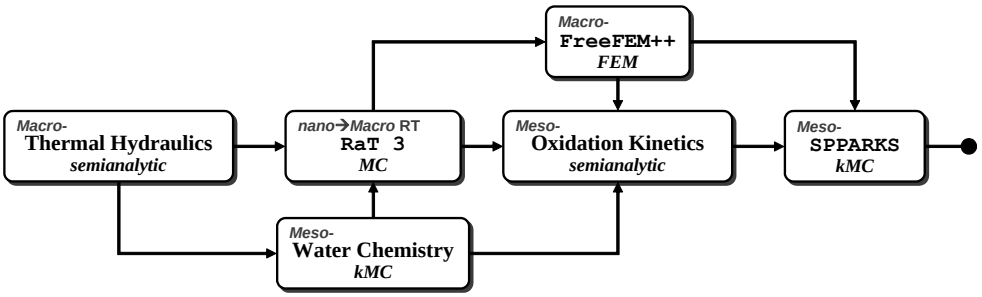

Fig. 5. The highest-level diagram of the MSMS computational sequence: tasks, methods, and software

2.1. SYSTEM THERMAL HYDRAULICS

STH modeling result in evaluation of the steady-state mass-flow rate W and profiling of circulating coolant properties (Fig. 6) base on standard U.S. NIST approved data on the Equation of State (EoS) and kinetic properties (*e.g.*, viscosity) of water.

Fig. 6 data are clear. The coolant speed is maximal inside the IC due to its relatively smaller hydraulic section. Water is mostly heated (and, thus, accelerated) just inside the IC due to EB power deposition Q_{beam}. It mainly occurs via heat transfer from dense hot walls of piping, cartridges and coupons. Water density sharply decreases with temperature just in the vicinity of the supercritical transition $T \rightarrow T_{pc}(P)$. This feature is known [1] to have its own impact on alloys corrosion.

2.2. COMPUTATIONAL DOSIMETRY

The results of the RaT 3.1 code MC RT modeling are used in several ways. First, the comprehensive database of absorbed dose and dpa was obtained on a *per sample* basis with high (~ 10 μm) spatial resolution and extended to the adopted scheme of samples cutting for further analysis.

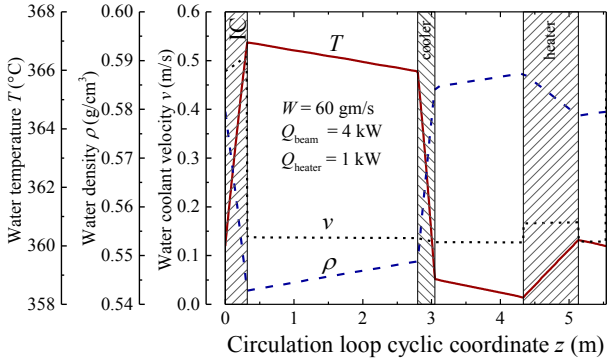

Fig. 6. Circumferential profiles of coolant speed, temperature and density. Its path length z in the circulation loop of Fig. 1 is counted from the IC bottom

An example of this procedure is presented in Fig. 7. It serves as a guideline for subsequent post-irradiation investigations [7] and assists in location of the most attractive Regions of Interest.

Besides, the RaT code outputs serve as power and ionization rate source terms for heat transfer and radiolysis kinetic equations which are solved by means of the greater scale methods, particularly by FEM. Their results (*e.g.*, the maps of temperature T_s) are also included into the sample inventory database as shown in Fig. 7.

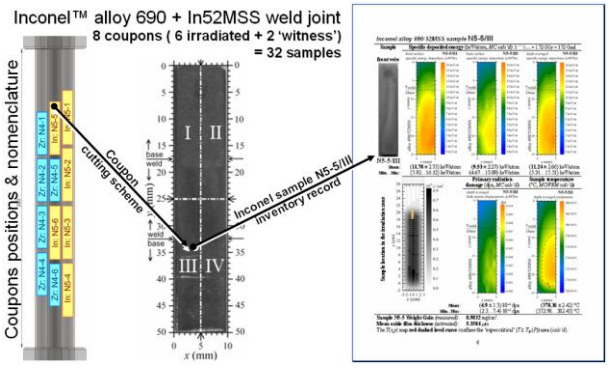

Fig. 7. Computational dosimetry based inventory of irradiated coupons: dose (keV/atom: front surface, rear surface, depth averaged mean value); primary radiation damage (dpa); temperature T_s; GCT measured δm/S. Data for alloy 690 sample No 5 part III

2.3. COMPUTATIONAL THERMOMETRY

Since temperature plays an essential role in corrosion phenomena, it has to be evaluated in great detail. Thermal-hydraulic, radiation transport and FEM calculations are applied consistently to obtain the sufficiently granular description of the corrosion environment. This has to be done for both the IC hardware (*e.g.*, pipes) and coolant as it is illustrated in Figs. 8 and 9, respectively.

In Fig. 8, the hottest (up to 463 °C) part of the IC is considered. FEM calculations point to the significant circumferential inhomogeneity of the temperature field.

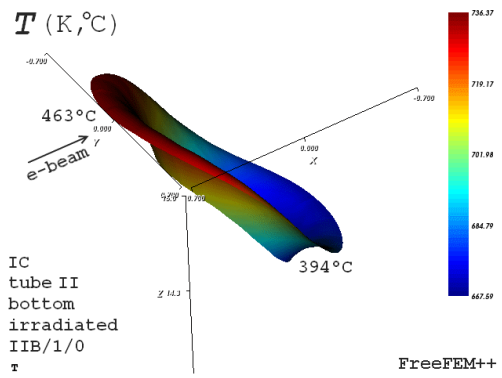

Fig. 8. 2D distribution of the SS 12X18H10T made IC tube #II temperature in the bottom part of the IC: STH → MC RT → FEM calculation procedure

The profiling of coolant temperature (see Fig. 9) reveals notable disparity of different IC tubes subject to their content and location *wrt.* the linac e^--beam. The water heating is the most strong and fast in the frontal tube No II. In the symmetrically positioned lateral tubes No I, III, water is nevertheless heated differently, stronger in the tube No I loaded with more dense and thick Inconel coupons. In the rear tube No IV, the EB deposited power is minor, and instead water is cooled due to the prevalence of heat loss to the environment.

Obviously, such finely resolved temperature fields cannot be directly measured experimentally since there is no chance to insert a sufficient number of operable calibrated thermocouples into the irradiated part of the circulation loop. MSMS has allowed to obtain it base only on the measurable temperature T_{in} at the IC inlet.

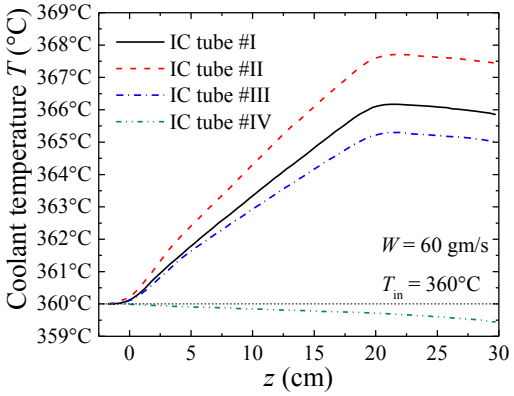

Fig. 9. Coolant temperature profiling per each of the IC tubes: STH → MC RT → FEM calculation procedure

2.4. STRESS-STRAIN STATE EVALUATION

FEM calculation of stress fields (Fig. 10) accounts for both internal pressure of coolant (23.5 MPa) and thermal-elastic stress due to the EB induced non-uniform heating. The obtained picture is rather complex and will be discussed more deeply in Section. 4.2.

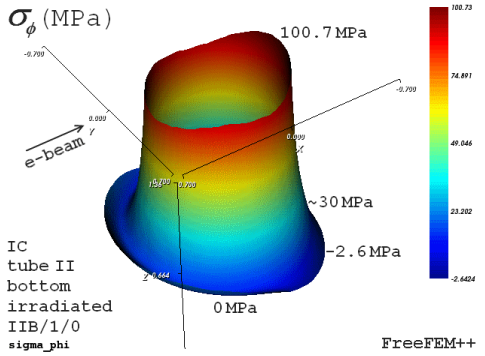

Fig. 10. 2D diagram of the FEM calculated hoop stress σ_ϕ in the bottom part of the IC tube #II (cf. Fig. 8)

2.5. COOLANT RADIOLYSIS SIMULATION

Our recently reported [18] MSMS of the coolant radiolysis in the SCWNCL was coupled to the E.I.T.F. experiment dose rate calculations (8.76 kGy/s in water). Radiolysis is itself of a multiscale nature. Its several stages at the successively increased timescale, from 10^{-15} s up to the exposure duration, were modeled consistently.

The production of radiolysis primary species (Fig. 11) was Monte Carlo calculated by application of the GEANT4–DNA Project [16] technique properly extrapolated to temperatures $T \sim T_c$. The validation against the up-to-date database [17] has shown good agreement with reference values characteristic for low Linear Energy Transfer (LET) irradiation.

Kinetics of radiolysis at the representative timescale of the E.I.T.F. experiment (~ $10^{1\ldots2}$ h) was calculated by numerical solution of the coupled system of spatially homogeneous stiff kinetic equations. Six primary species, 13 secondary ones and 46 reactions of 1st and 2nd order were modeled. Reaction constants were taken from ref. [17]. The characteristic results are given in Fig. 12.

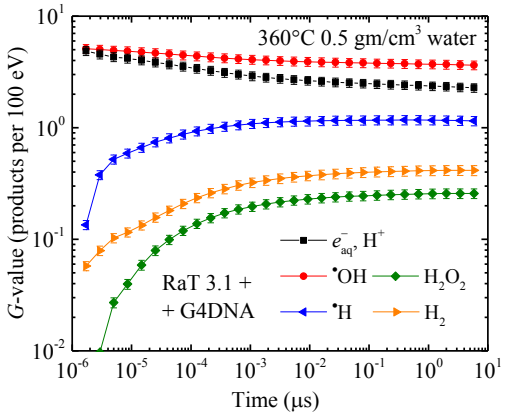

Fig. 11. Calculated primary specific yields of several major products of water radiolysis (G-values)

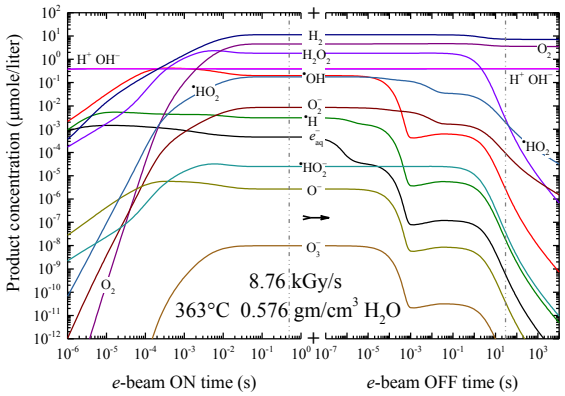

Fig. 12. Kinetics of immediate accumulation and successive 3-h-long relaxation of the radiolysis products

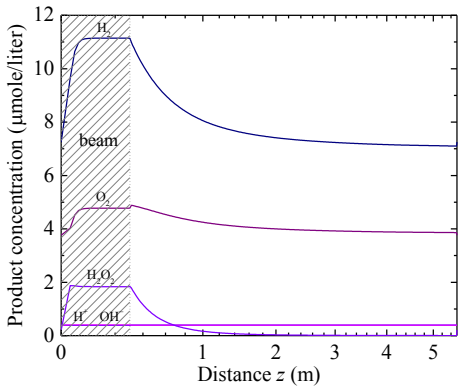

Fig. 13. Circumferential steady-state profile of the content of major relatively stable radiolytic species across the coolant path length z in the SCWNCL (cf. Fig. 6)

After the EB switching-on, the concentrations of radiolytic species immediately (in ~ 0.1 s) tend to equilibrium values. This does not change significantly the pH of water but results in a considerable increase of the dissolved oxygen (DO) content. The relaxation kinetic after the beam shutdown is more complex and prolonged. The relaxation time is of order of 10 s and is smaller than the STH derived coolant circulation period, ≈ 33 s. For this reason, coupling of the calculated kinetic kernels to the STH scenario (see Fig. 6) of coolant circulation results in the specifically varying steady-state profile of quasi-stable radiolytic products shown in Fig. 13.

Fig. 13 data describe quantitatively an indirect driving force of the irradiation assisted corrosion, the e^--beam induced enhancement of the content of essential corrodents (like DO O_2 and hydrogen peroxide H_2O_2) in the samples circumfluous coolant of the SCWNCL. It remains only to note that due to coolant flow interfusion, the proper effect of radiolysis on corrosion and oxidation is the same for all coupons in the irradiation cell.

2.6. THE REVEALED CORRELATIONS

An all-round analysis of the MSMS data has let us in on certain valuable correlations of the irradiation experiment environmental parameters. They are summarized in equations (1) below. An example is drafted in Fig. 14.

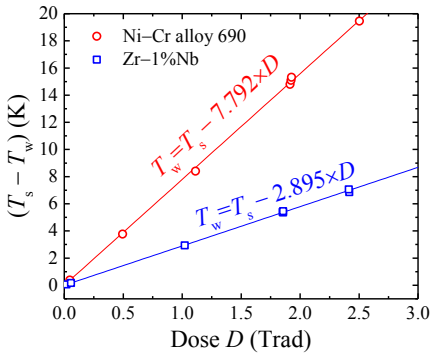

Fig. 14. Sample-coolant temperature difference correlations to the dose D absorbed in a sample

Such linear correlations are well conditioned:

$$T_s - T_w = \kappa_s D_s, \quad (1.1)$$

$$D_w = \kappa_w D_s, \quad (1.2)$$

$$N_{dpa} = \kappa_{dpa} D_s, \quad (1.3)$$

$$\rho_w \approx \bar{\rho}_w - \kappa_{\rho_w} \times \left(T_w - \bar{T}_w\right), \quad (1.4)$$

$$v_w \approx \bar{v}_w + \kappa_v \times \left(T_w - \bar{T}_w\right). \quad (1.5)$$

Here $T_{s,w}$ and $D_{s,w}$ are the temperatures and absorbed doses characteristic of a sample and of its immediate water environment of density ρ_w and speed v_w; N_{dpa} is a sample primary radiation damage estimate by a specific number of point defects; overlined quantities mean those averaged over the IC length.

Coefficients κ_i ($i \in$ s, w, dpa, r, v) were calculated and applied to the subsequent analysis of experimental data.

3. RESULTS AND DISCUSSION

3.1. IRRADIATION-ASSISTED CORROSION

The revealed correlations simplify the lookup of the IAC regularities since they allow to reduce the number of control state variables. Though both direct and indirect irradiation agents co-operate, they were found to be highly correlated. Thus, the problem of choosing the principal ones is largely a matter of agreement. We eventually settled on the choice of the sample absorbed dose $D = D_s$ and the local-to-sample water temperature T_w to be treated as direct qualifiers (Fig. 15).

In Fig. 15, a bi-linear trend is readily revealed for rather highly irradiated samples ##1–6 of both alloys:

$$(\delta m/S) = B \cdot (T_w - T_0) + C \cdot D. \quad (2)$$

'Witness' samples No 7, 8 irradiated to much smaller absorbed doses evidently drop out of this trend. Therefore, it can be attributed to the irradiation effect. Despite of a limited dataset, the reduced $\chi^2 \sim 10^{-(9\ldots8)}$ of the GCT data fit (2) is encouraging. It is remarkable that dose D and corrodent temperature T_w effects are in fact decomposed at least to the 2nd approximation (the terms $\propto D \cdot T_w$ are too small to stand out against a background of data statistical scattering). Therefore, variables (D_s, T_w) are acceptable as Principal Components (at least, in the statistical meaning of this term) and the coefficients (B, C) can be treated as fundamental temperature and dose sensitivities of the corrosion of materials.

As it is seen in Fig. 15 insets, the best-fit value of the temperature sensitivity factor B is 191 μg·cm^{-2}·K^{-1} for Inconel vs. 92 μg·cm^{-2}·K^{-1} for Zr-based alloy. Ni-Cr alloy 690 oxidation is about twofold more sensitive to the corrodent temperature; this promotes the KIPT fabricated Zr-1%Nb alloy to have higher 'thermal stability'.

Opposite, the irradiation dose sensitivity coefficient C of alloy 690, 239 μg·cm^{-2}·Trad^{-1}, amounts to almost half of that of the Zr-1%Nb alloy, 435 μg·cm^{-2}·Trad^{-1}. This suggests Inconel™ grade alloys to be more irradiation resistant in comparison with Zr-based alloy.

Indeed, these speculations are preliminary and require further experimental confirmations. Nevertheless, they are first based on a firm quantitative background.

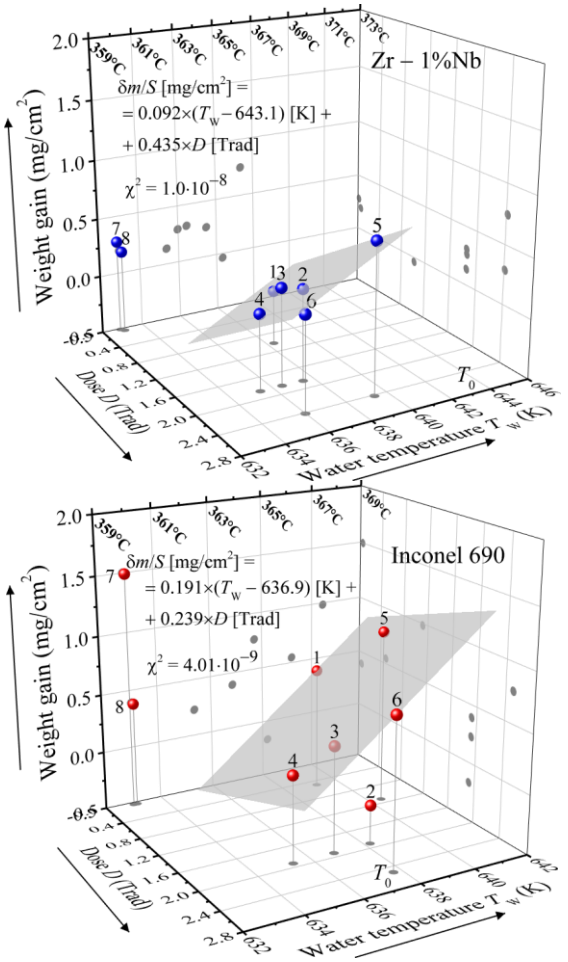

Fig. 15. Scatter plots of the Fig. 2 GCT δm/S data vs. the chosen corrosion control variables $D \equiv D_s$ and T_w

Thus, the following regularities of the alloys IAC was revealed: at e^--irradiation up to ≈ 2.5 Trad absorbed dose in the vicinity of the water supercritical transition at a circulating coolant temperatures 360…373 °C, for both Zr-1%Nb alloy and Ni-Cr-Inconel™ alloy 690, the alloys' corrosion/oxidation yield (i) increases linearly with dose at a fixed temperature, and (ii) increases linearly with temperature at a fixed dose.

To elaborate predictive models of alloys oxidation and corrosion in SCW under irradiation, the MSMS deduced empirical trend (2) has to be treated phenomenologically. Let us note that, due to eq. 2 bi-linearity, it can be agnostically represented as a sum of i-numerated bi-linear terms each of which is attributed to a certain driving force discussed in Section. 2.3:

$$(\delta m/S) = \Sigma_i\{B_i\cdot(T_w - T_{0,i}) + C_i\cdot D_s\}. \quad (3)$$

Such representation appeals only to the empirical sensitivities B and C which are known, from data fit, only as whole. Thus, one cannot find B_i and C_i unambiguously otherwise than by performing the i^{th} term dedicated measurements having all $j^{th} \neq i$ terms parameters fixed.

However, the same bi-linearity of (2) suggests an alternative constructive mechanistic approach. We introduce phenomenological susceptibilities μ_i, partial derivatives of the observable on a control variable, so that

$$\frac{\delta m}{S} = \mu_s\cdot T_s + \mu_w\cdot T_w + \mu_{D_s}\cdot D_s + \mu_{D_w}\cdot D_w + \mu_{dpa}\cdot N_{dpa} + \mu_{\rho_w}\cdot \rho_w + \mu_v\cdot v_w. \quad (4)$$

By equating (4) and (2) and applying correlations (1) of state variables, the system of linear equations is derived to find susceptibilities μ:

$$\begin{cases} B = \mu_s + \mu_w + \mu_v\kappa_v - \mu_{\rho_w}\kappa_{\rho_w}; & (5.1)\\ C = \mu_s\kappa_s + \mu_{D_s} + \mu_{D_w}\kappa_w + \mu_{dpa}\kappa_{dpa}; & (5.2)\\ T_0 = \left[\left(\mu_v\kappa_v - \mu_{\rho_w}\kappa_{\rho_w}\right)\cdot\bar{T}_w - \left(\mu_{\rho_w}\bar{\rho}_w + \mu_v\bar{v}_w\right)\right]/B. & (5.3)\end{cases}$$

Though the system (5) is generally underestimated, certain partial closed phenomenological models can be easily derived from it knowingly reducing (5) to the exactly solvable form for a subset of control variables. The obtained solutions form a basis for the further insightful analysis. We continue to work in this direction.

3.2. THE IRRADIATION-ASSISTED SCC ORIGIN

In ref. [7], the SS 12X18H10T corrosion was studied with two annual samples cut from the bottom and top parts of the IC frontal tube #II, Fig. 16. The bottom sample IIB/1/0 was highly (up to 14 keV/atom) irradiated and heated up to ≈ 460 °C. The top sample IIB/4 was situated out of the irradiation zone a little above 360 °C.

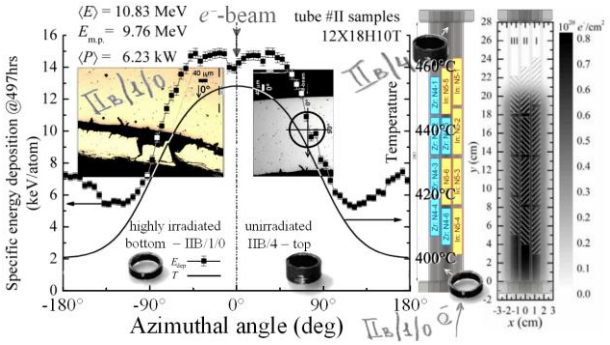

Fig. 16. Experimental details and preliminary characterization of the SS 12X18H10T annular samples [7]

In addition to the irradiation damage to ~ $6\cdot10^{-3}$ dpa induced ~ 30% hardening, the bottom sample metallography exhibited severe corrosion damage, right up to the exfoliation of the internal surface contacted with water. IGSCC was clearly identified inside and just behind the delaminated layer. In contrast, only a rough oxide film was found in the top sample along with certain traces of weak crevice corrosion but without any SCC.

Our MSMS FEM calculations have allowed to qualify quantitatively and to clarify the origin of the observed significant distinction in corrosion behavior of these samples. This is explained in Figs. 8, 10, and 17 in which the annular profiles of the relevant quantities are presented as functions of the azimuth $\phi \subset [-\pi, \pi]$ counted from the linac scanning EB symmetry axis $\phi \subset 0°$.

The main reason of a qualitatively different corrosion behavior lies in an uneven heating of the bottom sample (see Figs. 8 and 16, 17) caused by the azimuthally varying absorption of the EB power (see Fig. 16) in it. In Fig. 17, the FEM calculated temperature diagram of the top sample IIB/4 is fairly uniform and axially symmetric since no other heat source except of the coolant-to-pipe heat transfer exists for it. On the other hand, the ≈ 40 K high difference in temperature between the front (0°) and rear (±180°) surfaces of the bottom sample IIB/1/0 takes place, with maximum gradient $\nabla_\phi T$ on the sides ±90°. The EB induced temperature gradients immediately give rise to a thermal-elastic stress.

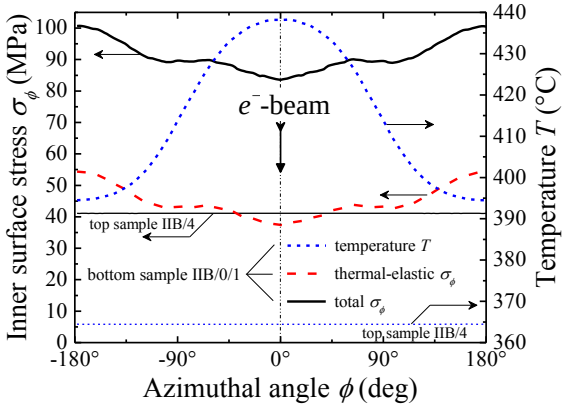

Fig. 17. Circumferential temperature and hoop stress profiles of the bottom (irradiated) and top (unirradiated) samples of the IC SS pipe

Stress FEM calculations were performed assuming standard mechanical properties of the 12X18H10T steel: Young modulus E = 200 GPa, Poisson's ratio μ = 0.30, linear thermal expansion coefficient $\alpha_T = 1.2\cdot10^{-5}$ K^{-1}. The elasticity-domain model is valid up to the temperature reduced yield stress $\sigma_{0.2}$ ≈ 178 MPa at T ~ 400 °C.

Figs. 10 and 17 represent the results of the tensile hoop stress FEM profiling of both samples at the static elastic relaxation of the internal pressure, 23.5 MPa. For the unirradiated sample IIB/4, the inner surface hoop stress $\sigma_\phi \approx 40$ MPa is axially uniform and has a reasonable value peculiar to the internal load of a thin tube. However, at the internal surface of the highly irradiated bottom sample IIB/1/0, σ_ϕ is about 2…2.5 times greater and increases from 85 MPa at the front side (0°) to 100 MPa at the rear (±180°) side of the sample.

The Fig. 17 dashed curve plotted auxiliary stress data (which were FEM calculated at zero internal pressure) definitely attribute the observed difference to the thermal elasticity effect. Thus, IGSCC of this sample is due to the contribution (≈ 40…50 MPa) of the indirect macroscopic effect of the irradiation, the thermal-elastic hoop tensile stress. One can conclude that the SS 12X18H10T IASCC activation threshold stress value exists and lies between 40 and 80 MPa. Dedicated experiments are required to refine this estimate. The mechanical stress effect on the corrosion behavior and SCC of prospective materials in SCW under irradiation is strong. This suggests a roadmap for further R&D.

4. CONCLUSIONS AND OUTLOOK

The NSC KIPT priority experimental data of *in situ* e^--irradiation of the topical GenIV SCWR Zr-, Ni-Cr- and Fe-Cr-based structural alloys are qualified quantitatively and explained theoretically by means of the consistent MSMS technique.

The bi-linear dependency of the Zr-1%Nb and Inconel 690 alloys corrosion/oxidation rate on the irradiation absorbed dose and water coolant temperature is first revealed. The phenomenological model approach to the evaluation of materials' sensitivity to the temperature and irradiation relevant corrosion agents is formulated.

The origin of the experimentally observed Inter-Granular Irradiation Assisted Stress Corrosion Cracking of the SS 12X18H10T material sample is evidentially attributed to the indirect irradiation effect, the thermal-elastic hoop stress. The existence of the IASCC activation threshold stress value is identified for the first time.

The developed MSMS technique is currently applied to the substantiation and computational support of the next-step *in situ* e^--irradiation experiments aimed at the investigation of corrosion under combined effect of supercritical water, irradiation, and mechanical stress load. Within the proposed and patented technique, the controlled bending stress is applied to the specimens in compliance with the developed scheme base on the sophisticated multi-scale calculations of stress diagrams and irradiation scenarios. The next generation target irradiation cell has been designed, manufactured, tested, and put into operation. The 500 h-exposure test irradiation of twenty SS 12X18H10T made bent samples in the SCW Circulation Loop was completed in September, 2019. Post-irradiation studies are in progress.

ACKNOWLEDGEMENTS

This work was partially supported by the Science & Technology Center in Ukraine Partner Project N 4841. It was also partially carried out at the expense of the budget program "Support for the Development of Priority Areas of Scientific Research" (КПКВК 6541230).

REFERENCES

1. D. Guzonas, R. Novotny, S. Penttila, A. Toivonen, W. Zheng. *Materials and Water Chemistry for Supercritical Water-Cooled Reactors.* Woodhead Publ. Ser. in Energy, Elsevier UK Ltd., Cambridge, 2018, 264 p.

2. G.R. Odette, S.J. Zinkle (Eds.) *Structural Alloys for Nuclear Energy Applications.* Elsevier Inc., Amsterdam, Oxford, Cambridge, 2019, 655 p.

3. *Accelerator Simulation and Theoretical Modelling of Radiation Effects in Structural Materials.* IAEA Nuclear Energy Series No. NF-T-2.2б ISBN 978–92–0–107415–7. IAEA, Vienna, 2018, 108 p.

4. J.A. Elliott. Novel Approaches to Multiscale Modelling in Materials Science // *Int. Materials Reviews.* 2011, v. 56, N 4, p. 207-225.

5. Ukraine Patent N 136862 (September 10, 2019). *Method of Investigating Corrosion Resistance of Structural Material Sample* / O.S. Bakai, V.M. Boriskin, R.M. Dronov, Yu.V. Gorenko, S.V. Shelepko, M.I. Bratchenko, S.V. Dyuldya.

6. A.S. Bakai, V.N. Boriskin, A.N. Dovbnya, S.V. Dyuldya, D. Guzonas. Supercritical Water Convection Loop for SCWR Materials Corrosion Tests under Electron Irradiation: First Results and Lessons Learned // *Proc. of the 6th Int. Symposium on SCWR's (ISSCWR-6),* March 3–7, 2013, Shenzhen, Guangdong, China. Paper N ISSCWR6-13062 (14 p.).

7. O.S. Bakai, V.M. Boriskin, A.M. Dovbnya, S.V. Dyuldya, D.A. Guzonas. Combined Effect of Irradiation, Temperature, and Water Coolant Flow on Corrosion of Zr-, Ni-Cr, and Fe-Cr-based Alloys // *Proc. of the ISSCWR-7*, March 15–18, 2015, Helsinki, Finland. Paper N ISSCWR7-2012 (14 p.); *J. Nucl. Eng. Rad. Sci.* 2016, v. 2, issue 1, 021007 (11 p.).

8. O.S. Bakai, V.M. Boriskin, M.I. Bratchenko, S.V. Dyuldya. e-Irradiation, Temperature, and Stress Effect on Corrosion of Zr-, Ni–Cr-, and Fe–Cr-based Alloys Near the Water Coolant Supercritical Transition // *Proc of the 5th Int. Conf. "High-Purity Materials: Production, Application, Properties",* Sept. 10–13, 2019, Kharkiv, Ukraine, p. 31-32.

9. P.R. Roberge. *Handbook of Corrosion Engineering.* McGraw-Hill, Inc., New York, San Francisco, Washington, D.C., U.S.A., 2000, 1128 p.

10. D. Feron (Ed.). *Nuclear Corrosion Science and Engineering.* Woodhead Publishing Series in Energy: N 22. Woodhead Publ. Ltd., Sawston, Cambridge, UK, 2012, 1042 p.

11. S.V. Dyuldya, M.I. Bratchenko. Methodology and Software for Multiscale Modeling of Radiation Impact on Materials: *Abstr. of XV Conf. "HEP. Nucl. Phys. Accelerators".* Kharkiv: NSC KIPT, 2017, p. 51-52.

12. S.V. Dyuldya, M.I. Bratchenko. Thermal Hydraulic Model of Natural Convection in the Super-Critical Loop of the NSC KIPT CU-EITF Facility // *Proc. of the ICPRP-XX*, Sept. 10–15, 2012, Alushta, Crimea, Ukraine, p. 50–51.

13. S.V. Dyuldya, M.I. Bratchenko, M.A. Skorobogatov. Novel Methods and Software of Statistic Modeling in Physics of Radiation Phenomena and Processes // *Proc. of the ICPRP-XVII*, Sept. 4–9, 2006, Alushta, Crimea, Ukraine, p. 30-31.

14. F. Hecht. New Development in FreeFem++ // *J. Numer. Math.* 2012, v. 20, N 3-4, p. 251-265.

15. S. Plimpton, C. Battaile, M. Chandross, et al. Crossing the Mesoscale No-Man's Land via Parallel Kinetic Monte Carlo: *SANDIA Report SAND2009-6226*, Oct. 2009; http://spparks.sandia.gov.

16. S. Incerti, M. Douglass, S. Penfold, S. Guatelli, E. Bezak. Review of Geant4-DNA Applications for Micro and Nanoscale Simulations // *Physica Medica*. 2016, v. 32, N 10, p. 1187-1200.

17. A.J. Elliot, D.M. Bartel. The Reaction Set, Rate Constants and g-Values for the Simulation of the Radiolysis of Light Water over the Range 20° to 350 °C: *AECL Report 153-127160-450-001,* Chalk River, Canada, 2009.

18. M.I. Bratchenko, S.V. Dyuldya. Multiscale Modeling of Coolant Radiolysis in the NSC KIPT Super-Critical Water Convection Loop under the LEU-10 Electron Linac Irradiation // *Abstr. of XVII Conf. "HEP. Nucl. Phys. Accelerators".* Kharkiv: NSC KIPT, 2017, p. 51-52.

Статья поступила в редакцию 27.11.2019 г.

ВЛИЯНИЕ ЭЛЕКТРОННОГО ОБЛУЧЕНИЯ, ТЕМПЕРАТУРЫ И НАПРЯЖЕНИЯ НА КОРРОЗИЮ СПЛАВОВ НА ОСНОВЕ Zr, Ni-Cr И Fe-Cr ВБЛИЗИ СВЕРХКРИТИЧЕСКОГО ПЕРЕХОДА ВОДНОГО ТЕПЛОНОСИТЕЛЯ

А.С. Бакай, В.М. Борискин, М.И. Братченко, С.В. Дюльдя

Количественные закономерности коррозии сплава Zr-1%Nb, Ni-Cr-сплава 690 и нержавеющей стали 12Х18Н10Т в околокритическом (23,5 МПа, 360…380 °С) циркулирующем водном теплоносителе разыскиваются с помощью многомасштабных расчетов показателей радиационного окружения эксперимента на сверхкритической водной конвекционной петле ННЦ ХФТИ под облучением электронами. Каждый из образцов количественно охарактеризован по дозе облучения, температуре, напряжению и измененным вследствие радиолиза химическим составом окружающего теплоносителя. Впервые выявлены и описаны в рамках предложенного механистичного модельного подхода билинейные увеличения прироста массы окисленных образцов с поглощенной дозой облучения и температурой коррозионного агента. Происхождение наблюденного в эксперименте коррозионного растрескивания стального образца объяснено вызванным облучением термоупругим окружным напряжением. Предсказано, что пороговое напряжение активации растрескивания лежит в пределах 40…80 МПа. Представлена экспериментальная методика исследования управляемой контролируемым напряжением коррозии в сверхкритической воде под облучением.

ВПЛИВ ЕЛЕКТРОННОГО ОПРОМІНЕННЯ, ТЕМПЕРАТУРИ ТА НАПРУГИ НА КОРОЗІЮ СПЛАВІВ НА ОСНОВІ Zr, Ni-Cr І Fe-Cr ПОБЛИЗУ НАДКРИТИЧНОГО ПЕРЕХОДУ ВОДНОГО ТЕПЛОНОСІЯ

О.С. Бакай, В.М. Борискін, М.І. Братченко, С.В. Дюльдя

Кількісні закономірності корозії сплаву Zr-1%Nb, Ni-Cr-сплаву 690 й нержавіючої сталі 12Х18Н10Т у білякритичному (23,5 МПа, 360…380 °С) водному теплоносії, що циркулює, розшукуються за допомогою багатомасштабних розрахунків показників радіаційного оточення експерименту на надкритичній водній конвекційній петлі ННЦ ХФТІ під опроміненням електронами. Кожний із зразків кількісно охарактеризований за дозою опромінення, температурою, напругою та радіолітично зміненим складом оточуючого теплоносія. Вперше виявлені й описані в межах запропонованого механістичного модельного підходу білінійні збільшення приросту маси окислених зразків з поглиненою дозою опромінення та температурою корозійного агента. Походження спостереженого в експерименті корозійного розтріскування стального зразка пояснене викликаною опроміненням термопружною окружною напругою та передбачено, що нижня гранична напруга активації розтріскування лежить поміж 40 і 80 МПа. Представлена експериментальна методика дослідження керованої контрольованою напругою корозії в надкритичній воді під опроміненням.